Annals of Work Exposures and Health, 2017, Vol. 61, No. 3, 311–320
doi: 10.1093/annweh/wxw031
Advance Access publication 9 January 2017
Original Article

Original Article

Characterization of Particulate Fume and Oxides Emission from Stainless Steel Plasma Cutting

Jun Wang*, Tien Hoang, Evan L. Floyd and James L. Regens

Department of Occupational and Environmental Health, College of Public Health, University of Oklahoma Health Sciences Center, 801 NE 13th St Room 425, Oklahoma City, OK 73104, USA

*Author to whom correspondence should be addressed. Tel: +1-405-271-2070 ext. 46767; fax: +1-405-271-1971; e-mail: jun-wang@ouhsc.edu

Submitted 7 June 2016; revised 27 October 2016; editorial decision 2 November 2016; revised version accepted 19 December 2016.

Abstract

Plasma cutting is a metal fabrication process that employs an electrically conductive plasma arc to cut metals. The metal fume emitted from stainless steel plasma cutting may consist of hexavalent chromium (Cr^{6+}), which is a carcinogen, and other toxicants. Overexposure to plasma cutting fume may cause pulmonary toxicity and other health effects. This study was to evaluate the effects of operation parameters (arc current and arc time) on the fume formation rates, Cr^{6+} and other oxides concentrations, particle size distributions (PSD), and particle morphology. A fume chamber and high-volume pump were used to collect fume produced from cutting ER308L stainless steel plates with arc currents varying between 20 and 50 A. The amount of fume collected on glass fiber filters was gravimetrically determined and normalized to arc time. Cr^{6+} and other oxides in the fume were analyzed using ion chromatography. PSD of the fume was examined using a scanning mobility particle sizer and an aerodynamic particle sizer for fine and coarse fractions, respectively. The particle morphology was imaged through a transmission electron microscope (TEM). Total fume generation rate increased with arc current and ranged from 16.5 mg min^{-1} at 20 A to 119.0 mg min^{-1} at 50 A. Cr^{6+} emissions (219.8–480.0 μg min^{-1}) from the plasma cutting were higher than welding fume in a previous study. Nitrogen oxides level can be an indicator of oxidation level and Cr^{6+} formation ($R = 0.93$). Both PSD measurement and TEM images confirmed a multimodal size distribution. A high concentration of a fine fraction of particles with geometric mean sizes from 96 to 235 nm was observed. Higher arc current yielded more particles, while lower arc current was not able to penetrate the metal plates. Hence, the worker should optimize the arc current to balance cut performance and fume emission. The findings indicated that arc current was the dominant factor in fume emission from plasma cutting. Appropriate ventilation and respiratory protection should be used to reduce workers' exposure.

Keyword: hexavalent chromium; plasma cutting fume; stainless steel; ultrafine particle

Introduction

Plasma cutting is a thermal cutting process that commonly used in the metal fabrication industry (Boekholt, 2000). It employs a high-temperature and energy-intense plasma arc to melt electrically conductive material, such as aluminum, brass, mild steel, and stainless steel (Ramakrishnan and Rogozinski, 1997). Figure 1 illustrates plasma cutting in both schematic and real-world images. During the arc-initiating period of plasma cutting, an inert gas or compressed air was blown out of the torch nozzle toward the workpiece. A pilot electrical arc forms and ionizes some gas, thereby creating a plasma channel capable of conducting electricity and providing a circuit. Once the plasma arc is established, the gas stops flowing, since it is unnecessary at this stage. This arcing process is in contrast to metal inert gas (MIG) welding, in which shielding gas is continuously flowing during the entire period of operation (Murphy *et al.*, 2009; Pocock *et al.*, 2009). The plasma arc moves across the workpiece surface and produces cuts in a short time. Compared with other thermal/non-thermal cutting process such as oxyfuel, laser, and water jet, plasma cutting is more versatile with higher penetration ability, less energy consumed, low consumable cost, and is highly mobile to perform work on different locations in the field (Krajcarz, 2014). Due to the aforementioned advantages, plasma cutting has been extensively utilized in all sectors, from large-scale industrial applications such as the oil/gas pipeline and vessel construction, to medium-scale metal salvage and scrapping, to small-scale home hobbyists. Many plasma cutting applications were performed on thick mild steel or stainless steel plates, where the capability of conventional cutting techniques is limited.

It is estimated that ~0.4 million workers in the USA are currently identifying themselves as welders (BLS, 2014) and 3 million people worldwide have welding and other metal fabrication as their main job duty (Pires *et al.*, 2006). Despite the efforts to mechanically automate the metal fabrication process, the number of workers exposed to metal fume is still growing continuously. The high energy and temperature process involved in metal fabrication draws concerns regarding the health risk from a variety of hazardous air pollutants. Similar to welding (Zimmer and Biswas, 2001), the high-temperature plasma arc vaporizes and oxidizes the components of workpieces and the surrounding gasses, including nitrogen, to form metal and nitrogen oxides (NO_x). The superior strength, mechanical properties, resistance to rust of stainless steel over carbon mild steel is due to the alloy's components (Marshall, 1984). Unfortunately, when thermal processes such as welding are performed on stainless steel, the alloying metals create toxic fume consisting of the metal in various oxidation states. The toxicity of chromium (Cr) is vastly different between its most common oxidation states: base (0), III (3+), and VI (6+). The most toxic to human health is hexavalent Cr (Cr^{6+}) (Kimura *et al.*, 1979). Other alloying constituents of concerns are nickel (Ni), and manganese (Mn) (Moroni and Viti, 2009), for whose toxicity are similar regardless of oxidation states and are typically measured as total elemental exposure. These toxic metals are either carcinogens (Cr^{6+} and Ni) or neurotoxins (Mn); all can produce serious detrimental health effects upon inhalation (Antonini *et al.*, 2003, 2006; Bowler *et al.*, 2006). More importantly, these particulate metals may be presented in submicron to ultrafine range (Hewett, 1995; Moroni and Viti, 2009). Depending on the particles' aerodynamic size and morphology, they are able to travel deeply into the respiratory tract to the alveolar region and, when small and soluble enough, they may become readily bioavailable to the circulatory system (Yu *et al.*, 2000; Biswas and Wu, 2005). Other safety and health

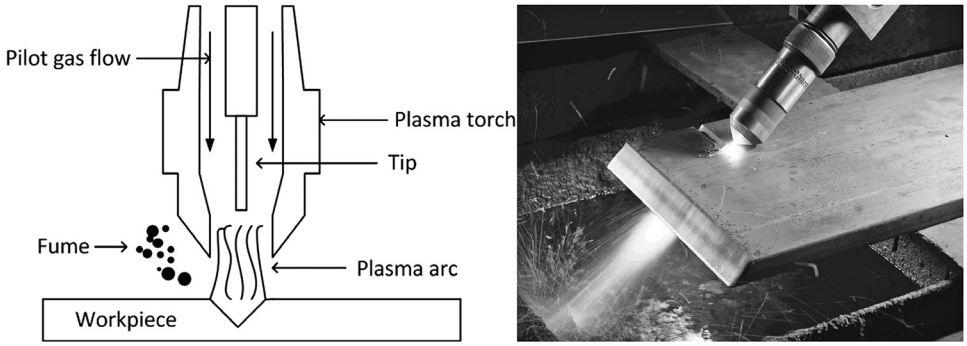

Figure 1. The structure of plasma cutting torch in schematic and real-world images. See Supplementary Figure 1 for color version at *Annals of Work Exposures and Health*.

concerns during plasma cutting include ultraviolet radiation and ozone formation from the plasma arc, which can lead to potential photokeratitis and skin burns of unprotected workers (Tenkate and Collins, 1997).

The chemical composition and inhalable fraction of the plasma cutting fume are theoretically determined by the type of metal being cut and the operation parameters. Although similar to welding in principles, the parameters governing plasma cutting (cutting speed, arc current) are different from welding (shielding gas, wire feed speed). It is well known that most welding fume comes from the vaporization of wire/filament/rod (Castner and Null, 1998), while plasma cutting fume should come from the base metal plate, since plasma cutting does not involve a consumable material. The absence of shielding gas flow may also increase fume emission and oxides formation, as there is no barrier for fume dispersion and cooling. In sum, it is critical to understand the correlations between the operation parameters and the fume emission of plasma cutting, not simply apply the knowledge learned from welding fume. While fume studies of conventional welding are abundant (Kimura *et al.*, 1979; Hewett, 1995; Castner and Null, 1998; Zimmer and Biswas, 2001; Pires *et al.*, 2006; Moroni and Viti, 2009), studies examining the characteristics of plasma arc cutting fume and health risks from exposure are limited (Oki *et al.*, 1994; Blunt and Balchin, 2002).

Currently, there is insufficient data on the physical and chemical characteristics of plasma cutting fume, leading to difficulty in regulations. The concern regarding exposure to these toxic metals, especially in nano- to micron-sized particles, was recognized long ago (Moroni and Viti, 2009). Various regulations and recommendations were made to limit the individual metal components in plasma cutting fume. The Occupational Safety and Health Administration (OSHA) made an 8-h time-weighted average (TWA) permissible exposure limit of 5 μg m^{-3} for Cr^{6+} (OSHA, 2006). The National Institute for Occupational Safety and Health (NIOSH) lowered the 10-h TWA recommended exposure limit (REL) for Cr^{6+} of 1 μg m^{-3} to the 8-h TWA REL of 0.2 μg m^{-3} in 2013 (NIOSH, 2008). NIOSH also recommended adoption of every reasonable control technology to further reduce Cr^{6+} in the workplace, due to the residual risk of lung cancer even at the most stringent REL (NIOSH, 2008). Although the American Conference of Governmental Industrial Hygienists (ACGIH, 2015) recommended a threshold limit value (TLV) of 50 μg m^{-3}, this value has not been updated since 2006. These efforts to tighten standards and recommendations highlighted that the previously set high value for Cr^{6+} was insufficient to protect workers. Meanwhile, all relevant agencies regulate or recommend exposure limits for Ni and Mn up to mg m^{-3} level, which are much more tolerable than those for Cr^{6+}.

To bridge the above-mentioned knowledge gaps, we investigated the chemical (Cr^{6+} and other oxides concentration) and physical (fume mass, particle concentration, size distribution, and morphology) properties of fume emitted from stainless steel plasma cutting. A welding chamber was utilized to collect the fume from cutting thick stainless steel plates. Multiple instruments were involved in characterizing the fume. Arc current was considered the primary variable, as it was directly linked to the energy and temperature of the plasma arc. Cr^{6+} exposure level and worst-case scenario estimation were compared with the existing limits. The ultimate goal of this study was to obtain an understanding of plasma cutting fume characteristics, compare these findings with existing welding fume data, and preliminarily assess the potential health risks associated with metal fabrication.

Methods

Fume chamber and plasma cutter

There are typically two ways to study the fume emission from a metal fabrication process, i.e. chamber sampling and personal breathing zone (PBZ) sampling, each with distinct advantages and disadvantages. Chamber sampling can collect a significant amount of fume mass in a short period due to the enclosed nature and efficient total capture design, thus making it possible to isolate and quantify the factors that affect the process more quickly. PBZ sampling is more physiologically relevant; however, the result is usually not readily replicable, and confounding factors often exist during the sampling. In the present study, a metal fume chamber was constructed according to the American Welding Society (AWS) specifications (AWS F1.2:2013) (AWS, 2006) as shown in Fig. 2. The galvanized steel-constructed conical chamber had dimensions of 30 inches at the base and 30 inches in height, with a tinted observation window and operator's glove holes on the chamber wall. A high-volume pump (Hurricane air sampler, Gelman Instruments, Ann Arbor, MI, USA) with a 90-mm filter holder was mounted on top of the chamber and operated at a flow rate of 0.5 m^3 min^{-1}. The flow rate was verified by a hot-wire anemometer (TSI 9545, Shoreview, MN, USA). Glass fiber filters (Whatman GF/A-90, Maidstone, Kent, UK) were used to collect particulate fume for later analysis. The high-volume flow pump was also used to purge the chamber and extract any residual fume between sampling sessions

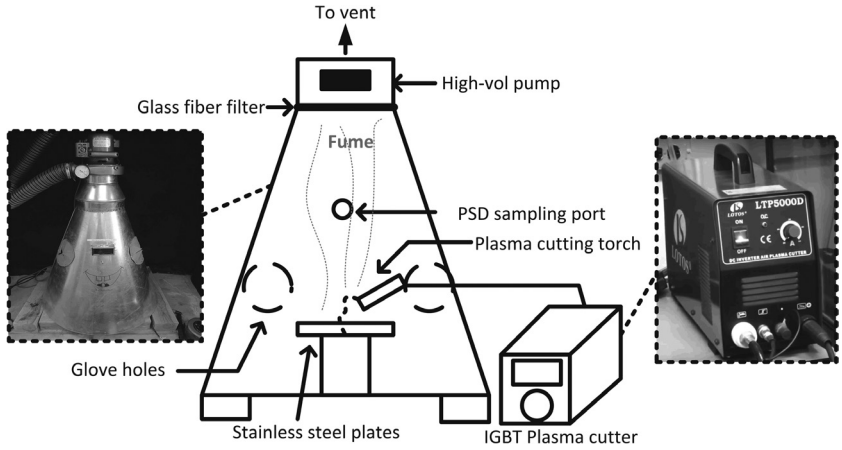

Figure 2. Schematic diagram of the sampling apparatus, with pictures of the chamber and the cutter shown on the left and right. See Supplementary Figure 2 for color version at *Annals of Work Exposures and Health*.

if any. The exhaust air was directed outside the building through ventilation.

An insulated-gate bipolar transistor (IGBT) plasma cutter (Lotos LTP5000D, Sunnyvale, CA, USA) was employed in this study, due to its popularity in the welders' community. IGBT was recently adopted by several plasma cutter manufacturers to promote cutting efficacy and capacity. An air compressor (Gast, Benton Harbor, MI, USA) supplied the pilot gas for the initial arc formation. The sampling factor matrix includes arc currents that were set on the plasma cutter between 20 and 50 A, and arc times of 5, 10, and 30 s, controlled by the operator using a stopwatch. Low-carbon stainless steel (ER308L) plates with a thickness of 4.8 mm (3/16 inch) were cut during the experiment. The ER308L stainless steel is composed of 18–20% Cr, 8–12% Ni, 2% Mn, 0.1% nitrogen (N), 0.045% phosphorus (P), and 0.03% sulfur (S), with the rest of mass mostly iron (Fe) (Vitek and David, 1987). A welder operated the plasma cutter through the glove holes and was later interviewed for more clarification of real-world practices of plasma cutting.

Determination of fume generation rate

The rate of fume emission was determined based on gravimetric analysis of the sampled filters. The filters were desiccated pre- and post-sampling in an isotemp oven (Thermo Scientific Precision 625, Waltham, MA, USA) and were weighed using an analytical scale (Mettle Toledo AG104, Columbus, OH, USA). The weighing difference was used to calculate the fume mass (mg) generated per sample using equation (1). We later found that the fume generated was linear related to the length of arc time (R^2 = 0.97). Hence, the fume generated was normalized to the arc time and aggregated per arc current:

$$\overline{\mathrm{FER}} = \frac{1}{3}\sum_{A}^{5,10,30s}\left(\frac{M_{\mathrm{post}} - M_{\mathrm{pre}}}{t}\right) \quad (1)$$

where $\overline{\mathrm{FER}}$ is the average fume emission rate (mg min^{-1}), m is the measured mass of filter pre- and post-sampling (mg), and t is the arcing time in minutes.

Chemical analysis of particulate Cr^{6+} and other oxides

The sampled filters, once weighed, were cut into halves for different extraction and analysis protocols. One half was used for Cr^{6+} analysis, while the other half was used for other inorganic oxides analysis. The average Cr^{6+} and oxides emission rate (μg min^{-1}) was calculated similarly to equation (1).

The Cr^{6+} analysis in this study followed a modified NIOSH Method 7604 (NIOSH, 1994). The half filter was heat-assisted extracted using 10 ml of a solution of 2% sodium hydroxide (NaOH) and 3% sodium carbonate (Na_2CO_3). The extracts were then analyzed using a conductivity-based ion chromatograph (IC; Dionex ICS-1600, Sunnyvale, CA, USA) equipped with an anion analytical column (Dionex AS4A, Sunnyvale, CA, USA) in the form of chromate (CrO_4^{2-}). The mass conversion of chromate to Cr^{6+} was done by multiplying a factor of 0.45 (the ratio of molecular weights of Cr^{6+} and CrO_4^{2-}).

Other particulate inorganic oxides, in the form of inorganic acids (e.g. NO_2 to NO_3^-), were determined based on the NIOSH Method 7903 (NIOSH, 1994). A solution of 1.7 mM sodium bicarbonate ($NaHCO_3$) and 1.8 mM Na_2CO_3 was used as extraction fluid

and eluent. Nitrous, phosphorus, and sulfur oxides were measured with the IC and anion analytical column, similar to Cr^{6+}. All results from IC analysis were doubled, since they were based on half of the sampled filter.

Particle size distribution measurement and morphology

A butanol-based scanning mobility particle sizer (SMPS; TSI 3936, Shoreview, MN, USA) in conjunction with an aerodynamic particle sizer (APS; TSI 3314, Shoreview, MN, USA) was used to obtain the particle size distribution (PSD) of the fume in the nanometer (nm) and micron (µm) ranges. A Y-connection to the PSD sampling port (Fig. 2) was utilized to split the sampled airflow to SMPS and APS. The SMPS sampled at a flow rate of 1.5 l min^{-1} and a sheath air flow of 3.0 l min^{-1} in the differential mobility analyzer column. This enabled a measurement of fine particles between 16.8 and 532.8 nm in 96 increments. The APS has a sampling flow rate of 1 l min^{-1}, with 4 l min^{-1} of sheath air flow simultaneously drawn from the sampling inlet and filtered. The scanning range of APS was between 0.542 and 19.81 µm in 50 increments, covering the coarse particle size range. The physical difference of electrical mobility size and aerodynamic size impeded a simple merger of SMPS and APS data. Hence, the PSD data were separately presented in the fine and coarse fractions, with geometric mean diameters (GMD) and geometric standard deviations (GSD, σ) reported.

Fume particles were also passively collected onto a lacey carbon film supported by polyvinyl formal resin (Pelco 300 mesh, Ted Pella, Redding, CA, USA). The film was held with a specially designed tweezer briefly inserted into the chamber through a sampling port. A transmission electron microscope (TEM; Hitachi H-7600, Schaumburg, IL, USA) was used to image the morphology of the fume particles that diffused onto the film.

Quality assurance/control and statistics

Methods limit of detection (LOD) were estimated and are listed in Table 1. All solutions and dilution used during analysis were made with deionized water from a filtration and ion exchange system (Barnstead Nanopure D11901, Waltham, MA, USA) to a conductivity of 18.2 mΩ cm. All chemicals were at analytical grade or higher in purity. The calibration curve for IC analysis was prepared by diluting stock solutions (Acros Organics, Morris Plains, NJ, USA) to an R^2 of 0.9999. Lab blank and spikes were used to monitor any signal shift from IC. Labware was mostly made of polytetrafluoroethylene to ensure that it was chemically inert, and was ultrasonically cleaned and dried prior to the experiment. The tubing used for plasma cutters was made of Tygon®, while the particle-laden tubing was made of conductive silicone to eliminate the electrostatic build up. Air leaking and flow tests were performed regularly.

Samples for each combination of arc current and arc time were performed in at least triplicate or more ($n \geq 3$). Results were expressed as mean ± standard deviation (SD). The effects of experimental factors were evaluated using two-way analysis of variance followed by the Tukey's multiple paired comparison test, with a significance level of $P = 0.05$.

Results

Total fume generation rate

Total fume generation rates increased with arc currents, as depicted in Fig. 3. The fume generation rates ranged from 16.5 ± 2.6 mg min^{-1} at 20 A arc current to 119.0 ± 38.7 mg min^{-1} at 50 A arc current. Differences in fume generation rates for each arc current were statistically significant, based on pairwise tests ($P < 0.05$). The fitting equation in Fig. 3 can be used to predict the fume emission level based on arc current, to an R^2 level of 0.75. Fume loading on the filter was also evidenced as a

Table 1. Analytical instruments and the corresponding LOD.

Measurement(s)	Instrument	LOD	Time resolution
Fume gravimetrical measurement	Analytical balance	0.1 mg per filter	Accumulated/continuous
Cr^{6+} in the form of chromate	IC	6.7 µg per sample	Accumulated/continuous
Inorganic oxides in the form of acids (PO_4^{3-}, SO_4^{2-}, NO_2^- and NO_3^-)	IC	1.0 µg per sample	Accumulated/continuous
Fine particles	SMPS	10^7 # cm^{-3} (upper) 10^3 # cm^{-3} (lower)	60 s
Coarse particles	APS	10^5 # cm^{-3} (upper) 10^{-2} # cm^{-3} (lower)	60 s
Particle morphology	TEM	10 nm	—

brown-orange color as pictured in Fig. 4a. The darker color of the sample filter increased with arc current indicating more carbon combustion products and metal oxides in the fume collected. High arc current provided more intense energy and promoted a deeper and cleaner cut, as shown in Fig. 4b. Cutting at 35–50 A arc current was able to penetrate completely through the back side of the plates, while 20–28 A barely left burn marks on the back side.

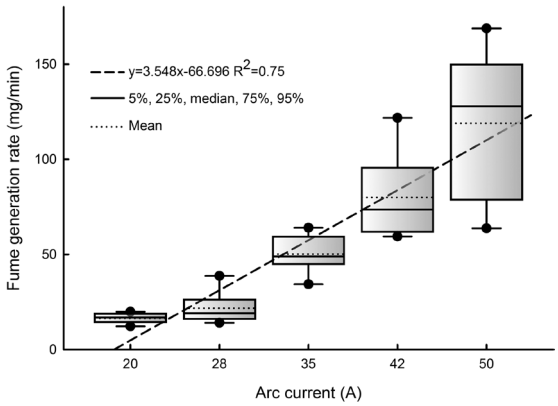

Figure 3. Fume emission rate (mg min^{-1}) as a function of arc currents (A) in box plot.

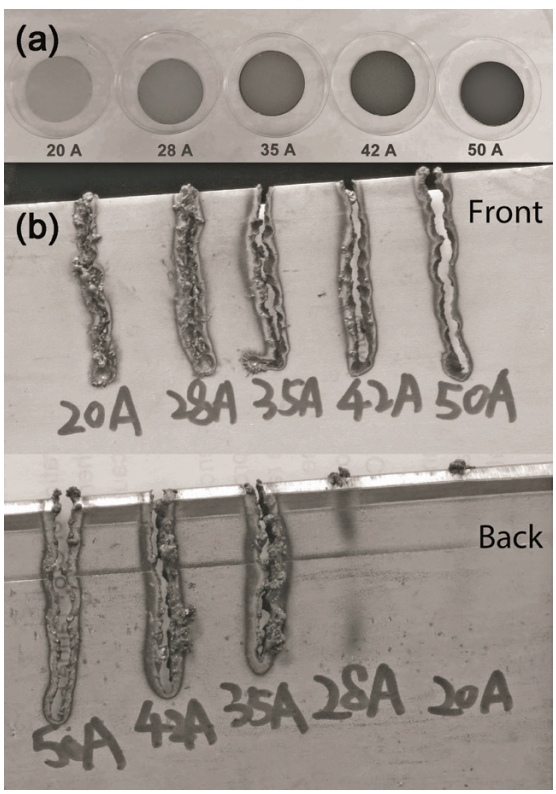

Figure 4. Pictures of (a) sampled filters and (b) cuts with different arc currents. See Supplementary Figure 4 for color version at *Annals of Work Exposures and Health*.

Particulate Cr^{6+} and oxides emission and exposure

The concentration of Cr^{6+} and other inorganic oxides in the fume should be directly correlated with the oxidation level. The oxidation reaction in the plasma cutting arc zone was not oxygen restricted, since there was no shielding barrier to prevent oxygen entry as is the case in welding. As presented in Fig. 5, Cr^{6+} emission rates averaged 219.8 ± 24.2 μg min^{-1} at 20 A arc current to 480.0 ± 49.6 μg min^{-1} at 50 A arc current. The only detectable inorganic oxides were NO_x in the forms of nitrate and nitrite (Fig. 5). The emission rates of nitrite ranged from 71.8 ± 2.3 μg min^{-1} at 20 A arc current to 150.6 ± 8.3 μg min^{-1} at 50 A arc current. Nitrate emission rates were statistically significantly higher than nitrite with a range of 86.3 ± 6.2 μg min^{-1} at 20 A arc current to 156.5 ± 6.8 μg min^{-1} at 50 A arc current. Trace amounts of phosphorus oxides and sulfur oxides were observed near the LOD in few samples.

PSD and morphology

The PSD measurement was consistent (coefficient of variation < 17%) for each arc current and was statistically significantly different across different arc currents ($P < 0.05$). Hence, the SMPS and APS results were averaged per each arc current, depicted in Figs 6 and 7 as particle number concentration (dN) in each size bin (dp) divided by base 10 logarithm of particle size [dN/dlog(d_p)], respectively. The single modal distribution ($\sigma < 1.8$) in the fine particle range with a shift of GMD was observed from 96 nm at 20 A arc current to ~235 nm at 50 A arc current. Fine particle concentration increased with arc current and reached a peak of 8.7 × 10^6 # cm^{-3} in the chamber at 50 A arc current. Results from the coarse particle measurement

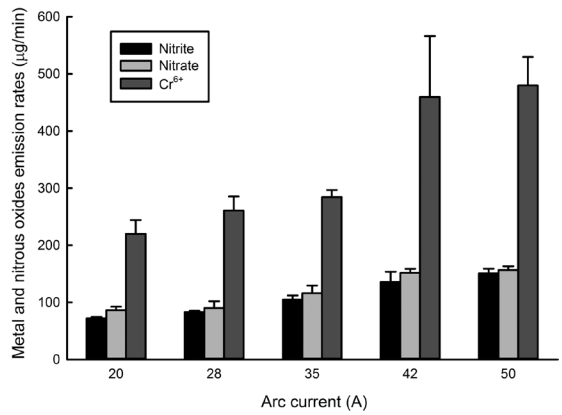

Figure 5. Cr^{6+}, nitrate, and nitrite emission rates (μg m^{-3}) as functions of arc currents.

indicated a bimodal distribution ($\sigma > 2.2$) with a much lower concentration. Similar to the fine particles, the highest coarse particle concentration (1.2×10^3 # cm^{-3}) was produced during cutting at 50 A arc current. However, the lowest coarse particle concentration (4.6×10^2 # cm^{-3}) was observed at the medium arc current of 35 A, instead of at the lowest arc current. As illustrated in Fig. 4, 35 A was also the lowest arc current that produced a clean cut without excessive energy input.

TEM images (particles generated from 35 A arc current presented in Fig. 8) supported the findings from SMPS and APS measurements, i.e. the existence of both ultrafine primary particles that were <100 nm and larger chain-like agglomerates formed from the inter-coagulation of fine particles. Some large spherical particles in the submicron range were also observed. The darker color resulting from high electron density to block the TEM electron beam indicated that those big spherical particles were primarily formed from the coalescence of metals.

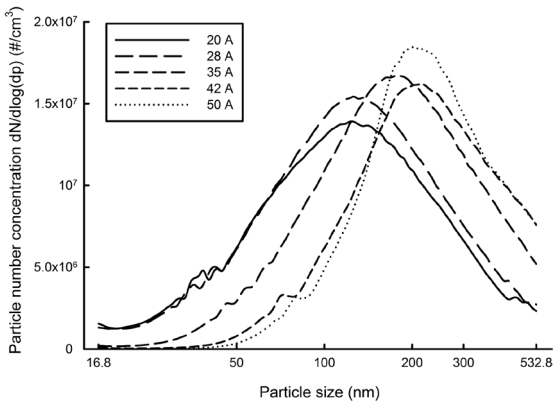

Figure 6. Fine particle distribution (dN/dlogd_p) based on concentration as a function of arc currents.

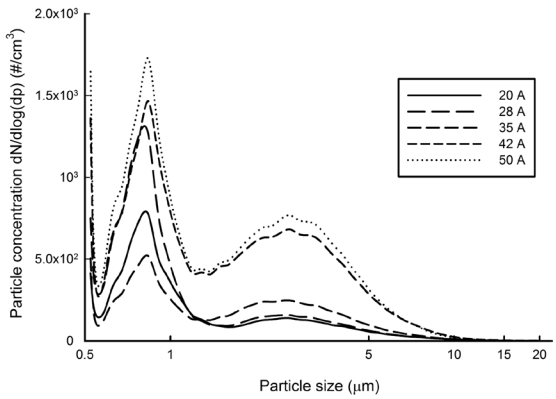

Figure 7. Coarse particle distribution (dN/dlogd_p) based on concentration as a function of arc currents.

Discussions

The results showed that arc current was the dominant factor affecting both chemical and physical properties of plasma cutting fume. Higher current equates to higher energy in the plasma arc, which led to more metal vaporization, more airborne particles, and a thermodynamic shift to favor oxidation. There was about seven times difference in the fume generation rate between the highest arc current (50 A) and lowest arc current (20 A). There is currently no regulation or recommendation from OSHA or NIOSH regarding metal fume. However, the American Conference of Governmental Industrial Hygienists (ACGIH) listed a TLV of 5 mg m^{-3} for welding fume (ACGIH, 2015). Using equation (2), the estimated fume exposure resulting from a high workload ($\gamma = 0.7$) can reach as high as 0.67 mg m^{-3}, which is still much less than the TLV. Hence, the total fume emission and exposure was not indicated as the primary concern of the present study.

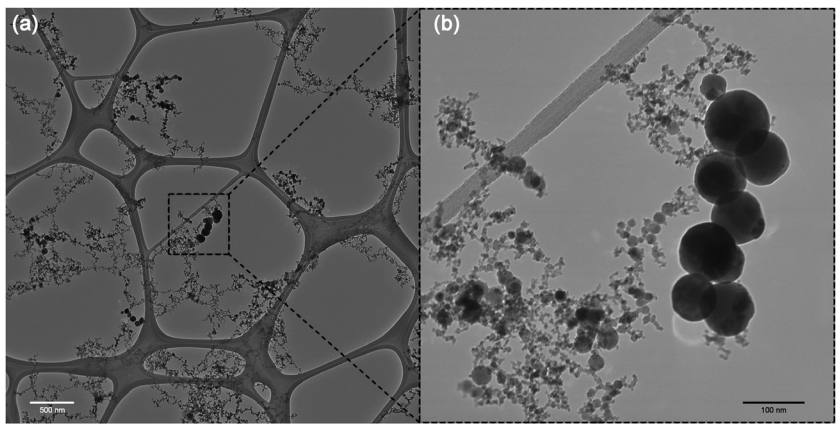

Figure 8. TEM images of fume particles <30 A arc current on (a) scale of 500 nm and (b) scale of 100 nm.

In general, the lack of shielding gas or shielded metal created an oxidation-rich environment that produced high levels of metal oxides, such as Cr^{6+}. The oxidation products of nitrogen in the surrounding air and stainless steel in detectable amounts can serve as an indicator of the availability of reactive oxygen species and oxidation levels. The high correlation coefficient (0.93) between Cr^{6+} emission and NO_x (nitrate + nitrite) emission suggested a strong positive correlation. A similar correlation was qualitatively observed in a previous study of welding fume (Dennis *et al.*, 2002). The analysis of Cr^{6+} in the workplace usually involves time- and resource-intensive sampling and lab work. By further studying the correlations between NO_x and Cr^{6+} in the field, a tool can potentially be developed to use NO_x gas monitors as prescreening or warning devices for Cr^{6+}. NO_x sensors or monitors are readily available and relatively low-cost either chemiluminescence or absorbance based. Trace amounts of phosphorus and sulfur existing in the stainless steel contributed to the material impurity, which was the reason that some PO_x (PO_4^{3-}) and SO_x (SO_4^{2-}) was detected at an ultra-low level.

A previous study (Wang *et al.*, 2012) of stainless steel welding with an identical AWS chamber setting showed that the Cr^{6+} generation rate was between 25 and 56 μg min^{-1} for gas metal arc welding. The Cr^{6+} emission rates in the present study were much higher, with a range between 219.8 and 480.0 μg min^{-1}. The difference between these two studies can be attributed to several factors: (i) the welding study employed a relative small home-use welder with a low capacity, while the IGBT plasma cutter used in the present study can feed energy at a much higher level; (ii) the thicknesses of working pieces were much thinner in the welding study (0.9 mm) versus 4.8 mm in this plasma cutting study, and (iii) the absence of shielding gases during plasma cutting to shield oxygen species from penetration, to blow away fume, and to disperse heat generated.

Both PSD and morphology images pointed out a multimodal distribution, with one mode in the fine fraction and two modes in the coarse fraction. The plasma arc created the 'hot zone' for metal vaporization. The metal vapor quickly condensed and formed numerous primary (fine) particles. The aggregation of fine particles that underwent inter-coagulation was seen in the TEM image. The higher arc current produced more fine particles and increased the fine mode GMD from 96 ng to 235 nm, which has lower respiratory tract deposition efficiency, based on the International Commission on Radiological Protection (ICRP) model (ICRP, 1994). However, when measured with an electrostatic classifier, the plasma-arc-generated particles could be either overcharged or have charge dispersion issue as studied by Chen *et al.* (2016). Hence, the results of SMPS measurement could be biased toward small particles and needs caution when using the qualitative results to calculating respiratory deposition efficiency. In the coarse particle fraction, mode sizes were stable with count concentration increasing with arc current, where the medium arc current (35 A) yielded the minimum particle concentration. Both high arc current (excessive energy and high particle concentration) and low arc current (metal pool formed, but no penetration) should be avoided in real-world practice. It should be noted that 35 A was the optimal arc current for this specific plasma cutter and particular plate thickness, and these recommendations may not be applied to different application scenarios. The worker should perform a trial cut to find the lowest arc current that can penetrate the metal. Feedback from interviews suggests that workers already follow this practice. Regardless of arc current, the concentrations measured in this study were of a higher magnitude (~10^7 # cm^{-3}) than observed in previous welding studies (10^5–10^6 # cm^{-3}) (Stephenson *et al.*, 2003; Lee *et al.*, 2007).

Conclusions

In the present study, we found that stainless steel plasma cutting fume contained high amounts of toxic metals, such as Cr^{6+}. The fume generation rates and oxidation levels were directly associated with the arc current. Higher arc current introduced more vaporization and fume formation, as well as oxidation. Although low arc current generally yielded lower fume emission, cutting could not be achieved at the lower end of arc current range. Thus, low arc current was not a viable option. These findings underscore the need for workers to exercise caution when selecting arc current to balance the job duty with fume exposure. It was worth nothing that the high positive correlation between NO_x and Cr^{6+} emission under the same arc current provides an alternative way to quickly determine Cr^{6+} concentration using a low-cost NO_x sensor and monitor in the workplace. However, a more in-depth quantitative field study is needed.

Particulate concentrations of both fine and coarse fractions were impacted differentially by arc currents. The high current arc created more fine particles, although it shifted the GMD to a larger one that is less favorable for respiratory deposition. In the coarse particle fraction, medium arc current produced fewer particles, since the excessive energy was avoided. TEM images confirmed the morphology of primary and agglomerate particles.

The findings point to the need for more experimental and field studies to verify exposure levels and varying operational parameters including personal exposure studies in the field to verify the exposure estimation method developed in the present study, determining concentrations of other toxic metals (Ni, Mn) in the plasma cutting fume, and *in vitro* and *in vivo* studies of plasma cutting fume toxicity.

Supplementary Data

Supplementary data are available at *Annals of Work Exposures and Health* online.

Acknowledgements

Funding for this research was supported by the Southwest Center for Occupational and Environmental Health (SWCOEH), a NIOSH Education and Research Center through grant T42OH008421. T.H. was a graduate student supported by the CDC/NIOSH industrial hygiene training grant T03OH008614. The authors thank the Oklahoma Medical Research Foundation (OMRF) for granting access to TEM and Mr Ben Fowler for assisting with the particle imaging. The authors appreciate Dr Chang-Yu Wu at the University of Florida providing stainless steel testing plates. The authors declare no other conflict of interest relating to the material presented in this article.

References

ACGIH. (2015) *Documentation of the threshold limit values and biological exposure indices*. Cincinnati, OH: ACGIH.

Antonini JM, Taylor MD, Zimmer AT *et al*. (2003) Pulmonary responses to welding fumes: role of metal constituents. *J Toxicol Environ Health A*; **67**: 233–49.

Antonini JM, Santamaria AB, Jenkins NT *et al*. (2006) Fate of manganese associated with the inhalation of welding fumes: potential neurological effects. *Neurotoxicology*; **27**: 304–10.

AWS. (2006) *F1.2:2006 laboratory method for measuring fume generation rates and total fume emission of welding and allied processes*. Miami, FL: American Welding Society.

Biswas P, Wu CY. (2005) Nanoparticles and the environment. *J Air Waste Manag Assoc*; **55**: 708–46.

BLS. (2014) *National employment matrix*. Washington, DC: U.S. Bureau of Labor Statistics.

Blunt J, Balchin NC. (2002) Fume, dust, vapour and gases. In Blunt J, Balchin NC editors. *Health and safety in welding and allied processes*. 5th edn. Abington, Cambridge, UK: Taylor & Francis. pp. 79–81.

Boekholt R. (2000) Welding and cutting systems, tools and supporting equipment and their influence on the workfloor environment. In Boekholt R, editor. *The welding workplace*. 1st edn. Abington, Cambridge, UK: Abington Publishing. pp. 73–82.

Bowler RM, Gysens S, Diamond E *et al*. (2006) Manganese exposure: neuropsychological and neurological symptoms and effects in welders. *Neurotoxicology*; **27**: 315–26.

Castner HR, Null CL. (1998) Chromium, nickel and manganese in shipyard welding fumes. *Weld J*; **77**: 223–31.

Chen BT, Schwegler-Berry D, Cumpston A *et al*. (2016) Performance of a scanning mobility particle sizer in measuring diverse types of airborne nanoparticles: multi-walled carbon nanotubes, welding fumes, and titanium dioxide spray. *J Occup Environ Hyg*; **13**: 501–18.

Dennis JH, French MJ, Hewitt PJ *et al*. (2002) Control of exposure to hexavalent chromium and ozone in gas metal arc welding of stainless steels by use of a secondary shield gas. *Ann Occup Hyg*; **46**: 43–8.

Hewett P. (1995) The particle size distribution, density, and specific surface area of welding fumes from SMAW and GMAW mild and stainless steel consumables. *Am Ind Hyg Assoc J*; **56**: 128–35.

ICRP. (1994) *Human respiratory tract model for radiological protection*. Ann ICRP, Publication 66. Ottawa, Ontario, Canada: International Commission on Radiological Protection.

Kimura S, Kobayashi M, Godai T *et al*. (1979) investigations on chromium in stainless steel welding fumes. *Weld J*; **58**: 195s–204s.

Krajcarz D. (2014) Comparison metal water jet cutting with laser and plasma cutting. *Procedia Eng*; **69**: 838–43.

Lee M-H, McClellan WJ, Candela J *et al*. (2007) Reduction of nanoparticle exposure to welding aerosols by modification of the ventilation system in a workplace. In Maynard, AD, Pui, DYH editor. *Nanotechnology and occupational health*. 1st edn. Dordrecht, The Netherlands: Springer Netherlands. pp. 127–36.

Marshall P. (1984) *Austenitic stainless steels: microstructure and mechanical properties*. London, UK: Elsevier Applied Science.

Moroni B, Viti C. (2009) Grain size, chemistry, and structure of fine and ultrafine particles in stainless steel welding fumes. *J Aerosol Sci*; **40**: 938–49.

Murphy AB, Tanaka M, Yamamoto K *et al*. (2009) Modelling of thermal plasmas for arc welding: the role of the shielding gas properties and of metal vapour. *J Phys D Appl Phys*; **42**: 194006.

NIOSH. (1994) *Method 7604: chromium, hexavalent by ion chromotography*.

NIOSH. (2008) *Criteria document update: occupational exposure to hexavalent chromium*. Cincinnati, OH: National Institute for Occupational Safety and Health (NIOSH), Division of Applied Research & Technology.

Oki Y, Numajiri M, Suzuki T *et al*. (1994) Particle size and fuming rate of radioactive aerosols generated during the heat cutting of activated metals. *Appl Radiat Isot*; **45**: 553–62.

OSHA. (2006) *Chromium (VI). Toxic and hazardous substances, Occupational Safety and Health Standards*. Washington, DC: National Institute for Occupational Safety and Health.

Pires I, Quintino L, Miranda RM *et al*. (2006) Fume emissions during gas metal arc welding. *Toxicol Environ Chem*; **88**: 385–94.

Pocock D, Saunders CJ, Carter G. (2009) *Effective control of gas shielded arc welding fume*. HSE RR 683. London, UK: Health and Safety Executive.

Ramakrishnan S, Rogozinski MW. (1997) Properties of electric arc plasma for metal cutting. *J Phys D Appl Phys*; **30**: 636.

Stephenson D, Seshadri G, Veranth JM. (2003) Workplace exposure to submicron particle mass and number concentrations from manual arc welding of carbon steel. *Am Ind Hyg Assoc J*; **64**: 516–21.

Tenkate TD, Collins MJ. (1997) Personal ultraviolet radiation exposure of workers in a welding environment. *Am Ind Hyg Assoc J*; **58**: 33–8.

Vitek JM, David SA. (1987) The aging behavior of homogenized type 308 and 308CRE stainless steel. *Metall Trans A*; **18A**: 1195–202.

Wang J, Kalivoda M, Guan J *et al*. (2012) Double shroud delivery of silica precursor for reducing hexavalent chromium in welding fume. *J Occup Environ Hyg*; **9**: 733–42.

Yu IJ, Kim KJ, Chang HK *et al*. (2000) Pattern of deposition of stainless steel welding fume particles inhaled into the respiratory systems of Sprague-Dawley rats exposed to a novel welding fume generating system. *Toxicol Lett*; **116**: 103–11.

Zimmer AT, Biswas P. (2001) Characterization of the aerosols resulting from arc welding processes. *J Aerosol Sci*; **32**: 993–1008.